Research Article

Journal of Geophysical Research: Oceans
DOI 10.1002/2017JC012797

A downslope propagating thermal front over the continental slope

by Hans van Haren[1], Phil J. Hosegood[2]

[1]Royal Netherlands Institute for Sea Research (NIOZ), P.O. Box 59, 1790 AB Den Burg, the Netherlands. e-mail: hans.van.haren@nioz.nl
[2]School of Marine Science and Engineering, University of Plymouth, Drake Circus, Plymouth, Devon, PL4 8AA, United Kingdom.

Received: Feb 13, 2017; Revised: Feb 13, 2017; Accepted: Mar 20, 2017

Abstract

In the ocean, internal frontal bores above sloping topography have many appearances, depending on the local density stratification, and on the angle and source of generation of the carrier wave. However, their common characteristics are a backwards breaking wave, strong sediment resuspension and relatively cool (denser) water moving more or less upslope underneath warm (less dense) water. In this paper, we present a rare example of a downslope moving front of cold water moving over near-bottom warm water. Large backscatter is observed in the downslope moving front's trailing edge, rather than the leading edge as is common in upslope moving fronts. Time series observations have been made during a fortnight in summer, using a 101-m long array of high-resolution temperature sensors moored with an acoustic Doppler current profiler at 396 m depth in near-homogeneous waters, near a small canyon in the continental slope off the Malin shelf (West-Scotland, UK). Occurring between fronts that propagate upslope with tidal periodicity, the rare downslope propagating one resembles a gravity current and includes strong convective turbulence coming from the interior rather than the more usual frictionally-generated turbulence arising from interaction with the seabed. Its turbulence is 3-10 times larger than that of more common upslope propagating fronts. As the main turbulence is in the interior with a thin stratified layer close to the bottom, little sediment is resuspended by a downslope propagating front. The downslope propagating front is suggested to be generated by oblique propagation of internal (tidal) waves and flow over a nearby upstream promontory.

Key Points: downslope frontal bore; Malin continental slope; internal fronts comparison

1. Introduction

One of the major contributors to the mechanical generation of turbulence in the ocean is the breaking of 'internal' waves [e.g., *Shrira*, 1981; *Gregg*, 1989]. Internal waves are mainly supported by the stable density stratification in the ocean interior. They can freely propagate when their frequency σ is in the range between the local inertial frequency $f = 2\Omega\sin\varphi$ at latitude φ and buoyancy frequency $N(x,y,z,t)$. This range generally includes tides, which are an important source of internal wave energy.

Generally just ocean-ward of shelf-breaks, the combination of a permanent pycnocline providing relatively large vertical density stratification (measured in terms of N) and relatively large vertical currents yields favourable conditions for the conversion of energy from surface to internal tides [e.g., *Baines*, 1982; *Munk*, 1997; *Gerkema et al.*, 2004]. Estimates of conversion rates vary considerably depending on the model used, see *Munk* [1997] for a discussion. Although mid-ocean ridges seem more important for energy conversion to internal tides, the conditions ocean-ward of the continental shelf breaks are not negligible especially considering 3D topography generation [*Gerkema et al.*, 2004], and because their slopes (β) are close to critical, i.e., closely matching the slope α of an internal wave ray given by $\sin^2\alpha(\sigma) = (\sigma^2-f^2)/(N^2-f^2)$, when $N >> f$ [e.g., *LeBlond and Mysak*, 1978].

Considerable internal wave breaking occurs at underwater topography, such as seamounts, continental slopes and small-scale hills [*Eriksen,* 1982*; Thorpe,* 1987*; van Haren et al.,* 2015]. In the open ocean away from topography, internal waves can be mainly linear and turbulence generation is generally very weak [e.g., *Gregg*, 1989]. The nonlinear features of incoming and reflecting waves above a sub-critical slope, $\beta < \alpha$ [*Thorpe*, 1992], and solitary waves of elevation [*Helfrich*, 1992; *Vlasenko and Hutter*, 2002] can develop as a turbulent front that moves up the slope (Figure 1). Besides in theoretical and numerical predictions, such front(al bores) have been observed in the laboratory over near-critical slopes [e.g., *Dauxois et al.*, 2004]. In the ocean, they have been observed at a variety of slopes ranging from sub- to super-critical (for internal tides) under different principal forcing varying from

internal tides to sub-inertial (non-internal wave) topographic waves [*Klymak and Moum*, 2003; *Hosegood and van Haren*, 2004].

The fronts have mainly been observed moving relatively dense (cold) water close to the boundary as they occur following the transition from down- to upslope phase of the principal carrier wave. They have an appearance that resembles the structure of a 'gravity current' [*Venayagamoorthy and Fringer*, 2007], despite the front propagating upslope. The associated backwards breaking and frontal shape differs for all bores [e.g., *van Haren*, 2006]. Over complex topography of a canyon above a supercritical slope for semidiurnal tides in the Bay of Biscay, regular cold water fronts associated with the (main) upslope phase of the tide are found preceded by local upslope motions in the 30 min before, followed by local downslope flow after the frontal bore passage [*Gemmrich and van Haren*, 2001]. This was attributed to the gravitational collapse of internal waves propagating obliquely to the main slope.

In this paper, we present a rare downslope (propagating) front, which, compared to the more common upslope propagating front, has inverse temperature characteristics: a front upside down (Figure 1). During tidal periods before and after this event, multiple upslope propagating fronts are observed in the same area.

2. Materials and methods

We investigate a site where internal tidal wave generation and possibly breaking can be expected, just below the shelf break of the North-West European continental slope (Figure 2). For the duration of 15 days in July 2013, a temperature (T) sensor array was moored at 55° 54.230′N, 9°16.934′W, 396 m water depth as shown by the yellow dot in Figure 2. This site, off the Malin Shelf, demonstrates near-critical matching of bottom slope with semidiurnal internal tidal wave slope $\alpha(M_2)$. Using local shipborne Seabird 911-plus Conductivity Temperature Depth CTD-observations to evaluate N, we find around the depth of the moored temperature sensors $\alpha(M_2) = 0.06$ for mean $N = 1.2\times10^{-3}$ s^{-1} with a maximum of $\alpha(M_2)_{max} = 0.14$ for minimum $N_{min} = 5\times10^{-4}$ s^{-1}. Temperature dominated salinity in density variations

(Figure 3a-c). The relatively weak stratification compared to other shelf break sites is attributed to 'mode' water, a nearly vertically homogeneous water mass created by deep convection in winter. The estimated local bottom slopes are $\beta = 0.06 \pm 0.01$, with maximum $\beta = 0.09$, indeed approximately matching the above $\alpha(M_2)$.

A total of 102 NIOZ4 high-resolution T-sensors were taped at 1 m intervals to a nylon-coated 0.005 m diameter steel cable. The sensors were between 13 and 114 m above the bottom. Unfortunately, 27 sensors and thus their data were lost after the mooring was hit by a 'longliner' fisherman and torn from the line on the release of the anchor during recovery (see Figure 4a below for positions of these sensors). 1 metre above the upper sensor a downward looking 300 kHz four-beam TeleDyne/RDI Acoustic Doppler Current Profiler (ADCP) was mounted. The horizontal currents measured by the ADCP are decomposed in along-slope (15° from North) and cross-slope (15° from East) components. The relative acoustic echo amplitude 'dI' is computed with respect to its time mean for every 2 m depth level (vertical bin) of the ADCP. The 300 kHz dI gives some qualitative indication of resuspended sediment near sloping topography [*Hosegood et al.,* 2004], but we note that this may be partially mixed with stratified turbulence there [*van Haren*, 2007] whilst being most sensitive to 'particles' of sizes of a mm and larger [*RDI*, 1996]. It has not been calibrated and cannot provide a quantitative measure for (fine) sediment resuspension. The ADCP measured at a rate once per 15 s, which is here sufficient to obtain detailed information on phase propagation of fronts from the different arrival times in echo amplitudes of the beams [*van Haren*, 2007]. From that previous experiment by *van Haren* [2007], in which frontal phase speed c and direction estimates from echo amplitudes are compared with particle velocities $\mathbf{u}_p$, we know that they are highly aligned in direction within a range ±10°, while $|\mathbf{u}_p|_{max} = 1.6 \pm 0.4c$ and the frontal bores' particle speed $|\mathbf{u}_p|_{enc} \approx c$. We can therefore use the information on the directly measured particle velocities from ADCP to establish speed and direction of frontal propagation and compare with the inferred phase speed and direction of the front from the different times of elevated acoustic backscatter in opposing beams.

NIOZ4 are self-contained T-sensors sampling at 1 Hz, with precision better than 5×10^{-4}°C (after drift-correction) and a noise level of $<1\times10^{-4}$°C, see [*van Haren et al.*, 2009] for the predecessor 'NIOZ3' with similar characteristics. Every four hours, all sensors are synchronized via induction to a single standard clock, so that the entire 101 m range is sampled in less than 0.02 s. The T-data are converted into 'Conservative' (~potential) Temperature data Θ [*IOC, SCOR, IAPSO*, 2010]. The high sampling rate, at least 100 times faster than the highest internal wave (buoyancy) frequency, the large number of sensors and the high precision allow for detailed observations of internal waves and turbulence, also in weakly stratified waters. However, as we do not measure salinity with these sensors, the CTD data are needed to establish a temperature-density relationship in order to be able to estimate turbulence parameters. A constant linear temperature-density relationship is used with slope of -0.2, as established for the range between 300 and 400 m from CTD-observations (Figure 3d,e). Thus, turbulence estimates can be made using the method of computing vertical displacements d between original and reordered density (temperature) profiles as introduced by *Thorpe* [1977]. Hereby, N is computed from the reordered profiles. Averaging is done over the entire range of sensors instead of over single overturns. Single overturns are difficult to define as overturns of different sizes are found at any given time and depth. Two-hour, 101-m averaged values are used to compute the dissipation rate, $\varepsilon = a^2d^2N^3$, using a constant value of $a = 0.8$ for the Ozmidov/rms displacement ratio [*Dillon*, 1982]. For the eddy diffusivity $K_z = \Gamma a^2d^2N$, a constant mixing efficiency of $\Gamma = 0.2$ is used [*Osborn*, 1980; *Oakey*, 1982]. This is commensurate with nearly all oceanographic estimates of turbulence using the method of *Thorpe* [1977]. Further details for its use with moored temperature sensors is given in *van Haren and Gostiaux* [2012] and *van Haren et al.* [2015].

3. Observations

Interpretation of the present T-data set is a challenging task, because of the varying stratification. Portions of the data are in near-homogeneous waters. Such weak stratification is

generally more common in the deep ocean. Buoyancy periods of typically 5100 s (~1.5 h) and up to 12,000 s (>3 h) occur, the latter narrowing the internal gravity wave band $f < \sigma < N$ to only half an order of magnitude. The local inertial period is about 52,000 s (14.4 h).

An overview of the temperature throughout the fortnight in the lower 115 m above the bottom at the thermistor string mooring (Figure 4) shows a gradual increase in temperature, presumably due to an eddy or to the meandering of the slope current., whose core is between 200 and 300 m at the cross-slope position of the mooring. Superposed on the slow variation with time is the semidiurnal variation, best visible in the horizontal cross-slope current component (Figure 4b). This variability is also seen, albeit less dominant, in temperature (Figure 4a), along-slope current component, which is virtually always positive with mean speed of 0.19 m s^{-1} directed towards the north-northeast (Figure 4c), vertical current component (Figure 4d) and dI (Figure 4e).

In these four depth-time series, the semidiurnal variability is more non-sinusoidal than in Figure 4b. This is most manifest in a sudden transition from the warming (yellow-red) to the cooling (blue) phase of the tide in Figure 4a. In general such a transition is accompanied by a transition from down- (blue) to upslope (yellow-red) horizontal currents (Figure 4b), and regularly, but not always, by vertical motions and dI extending from the bottom upwards (Figure 4d,e). It occurs nearly every tidal cycle, although in varying intensity.

These transitions are the now commonly observed upslope propagating frontal bores that dominate sediment resuspension [*Hosegood et al.*, 2004]. A detail-example is given in Figure 5. The intensity and form vary strongly from bore to bore, here in this area as well as in others like in the Bay of Biscay [e.g., *van Haren*, 2006] occurring more or less, to within 10%, with the semidiurnal periodicity. They all have a cold-front that passes the mooring within minutes, the leading edge some 10-20 m from the bottom, being at least 50 m high and strongly turbulent, with a relatively strongly stratified layer higher-up moving vigorously up and down due to the turbulence. Upward ejection of fluid from the bottom occurs mainly around the frontal passage. The front is not a smooth rigid structure and extends above the range of T-sensors, as can be inferred from the unstable temperatures around z = -290 m, t =

186.56 yeardays. Such 'frontal instabilities' have been observed previously, see e.g., Figure 4 in [*van Haren*, 2007]. Averaged over the time-depth span of Figure 5, the mean turbulence values are $\varepsilon = 1 \pm 0.4 \times 10^{-7}$ m^{2}s^{-3}, $K_z = 3 \pm 1 \times 10^{-2}$ m^{2}s^{-1}.

An unusual exception is seen to occur on day 187.9 (purple line marked F6 in Figure 4a), when a transition to cold waters occurs during downslope (blue) flow (Figure 4b). The 2-h detail in Figure 6 shows a front, but which resembles more a gravity current as it appears upside down compared to the upslope moving front of Figure 5. For both fronts, the along-slope current was positive, directed towards the north-northeast, with an amplitude varying between 0.2 and 0.3 m s^{-1}; as the downslope front in Figure 6 passed the mooring, alongslope velocity increased from 0.16 m s^{-1} to 0.32 m s^{-1} within 35 minutes. The direction of propagation is inferred from the particle velocities and timing of elevated acoustic backscatter in the ADCP beams. Accounting for the ADCP heading and its mounting in a downward looking configuration, the trailing edge of the front within which the acoustic backscatter was highest passed beam 1, which was pointing towards 155°N, 293 seconds before the opposing beam 2 (Figure 7). The time of arrival of the trailing edge at beams 3 and 4 are difficult to distinguish, although beam 4 seems to be passed before beam 3, suggesting the direction of propagation to be between 310 and 335°N. At a range of 90 m, the beam spread equates to 64 m, indicating a phase speed of 0.21 m s^{-1}. The northwestward propagation, which corresponds to a poleward, downslope direction, is consistent with the particle velocities of 0.32 m s^{-1}, such that $|\mathbf{u}_p|_{max} = 1.5c$, that were directed towards 340°N.

Although being a cold-front, the leading edge is some 80 m above the bottom in Figure 6. This is several tens of meters higher than for typical upslope moving frontal bores. It appears as a bottom separation, as sketched in Figure 1 lower-right, and which is possible in turbulent overturns over a span of time that is smaller than the local buoyancy period. The relatively warmer waters below are progressively closer to the bottom and move slightly slower off-slope than the cooler waters above. This unstable density configuration facilitates convective turbulence. Averaged over the time-depth span of Figure 6, the mean turbulence values are ε

$= 5\pm2\times10^{-6}$ m^2s^{-3}, $K_z = 3\pm1\times10^{-1}$ m^2s^{-1}. The Rayleigh number amounts $Ra = g\alpha/\nu\kappa\cdot\Delta TL^3 \approx 5\times10^{14}$ for a range of sensors L = 100 m, and a temperature difference of $\Delta T = 0.05$ K. Here, g denotes the acceleration of gravity, α the thermal expansion coefficient, ν the kinematic viscosity and κ the thermal diffusivity. The large Ra > 1000 indicates that turbulent convection dominates conduction [*Allaby and Allaby*, 1999]. From laboratory observations in a porous medium, *Lister* [1990] found for Ra > 1000 a significant number of dendritic downwellings eventually feeding into a single downwelling plume. Here, plumes seem to be more extending upwards, away from the bottom. Given the large Ra and an estimated Rossby number > 1, the flow regime is characterized by turbulence rather than geostrophic turbulence in which rotation effects are important [*Boubnov and Golitsyn*, 1990; *Marshall and Schott*, 1999].

Such turbulence has similar small-scale overturn features to that for upslope bores but it is found to last a much longer period of 2 h compared to several minutes during upslope bores. This 2-h period is still smaller than the maximum buoyancy period and motions thus can last being unstable, and turbulent, as was also found for Rayleigh-Taylor mixing by [*Lawrie and Dalziel*, 2011]. Motions with periods longer than the buoyancy period, like internal waves, need to be in a stable environment for support. Also in contrast with Figure 5, the upwards ejection of fluid from near the bottom does not occur at the front at day 187.88 in Figure 6, but later at day 187.94 when the colder layer reaches the bottom from above. This was the only example of a downslope moving front observed in the 15 day record, although on two occasions much weaker quasi-upside down fronts were observed during slack-water, when the cross-slope current was almost zero, and one occasion with vigorous cold-water convective overturning from above without a propagating front.

4. Discussion and conclusions

The observed gravity current resulting in a downslope moving frontal bore is an unusual exception to the now commonly observed upslope moving bores above deep-sea topography

[e.g., *Klymak and Moum*, 2003; *Hosegood et al.*, 2004]. Although the latter are known for their impact on sediment resuspension [*Hosegood et al.*, 2004; *Bourgault et al.*, 2014], such resuspension is unknown for the former. The associated turbulence trailing the downslope propagating bore has a different character, principally coming from the interior and being strongly convective rather than shear-induced.

Judging from turbulence estimates, the upside down front is an order of magnitude more turbulent than regular, upslope propagating frontal passages. Variations in the value of the slope in the local temperature-density relationship are observed, but we note that this does not raise doubts about the static stability of the front in Figure 6, as the sign of slope is always negative.

The mechanism for generating the gravity current leading to the downslope moving frontal bore seems associated with the canyon, or the oblique propagation of the large-scale carrier wave along the continental slope, here the semidiurnal internal tide. No difference is found in the large-scale along-slope directed current between upslope and downslope frontal passages. The rare occurrence of the latter seems thus more related with a gravitational collapse, rather than with a local change in slope-current. In contrast with the findings in the Bay of Biscay [*Gemmrich and van Haren*, 2001], the present downslope front is not preceded by upslope motions in the 30 min before the frontal passage.

As for the consequences for ocean mixing, underwater topography should be considered in full 3D as the flow-effects of promontories and canyons seem to be important. Numerical modeling results from a shelf break region in the Celtic Sea indicate that internal tides generated at submarine promontories, similar to that found upstream of the current mooring location, spread radially from their source region [*Vlasenko et al*., 2014]. Baroclinic internal tidal energy thus propagates along the slope rather than primarily across it, raising the possibility that the predominant along-slope velocity, rather than the usual cross-slope dominance, in the bores observed here is attributable to remotely generated internal tides. Recent modelling results further indicate the potential of tidal flow over the same promontory discussed here in generating along-slope propagating bottom trapped internal waves

[*Stashchuk and Vlasenko*, 2017]. The waves in the modelling case intensified currents over the lower 400 m, approximately, in water of depth 1000 m. This is somewhat deeper than the fronts observed in our observations but the constant and time-independent stratification used in the model suggest that such a mechanism may be implicated when realistic variability in background stratification, such as that observed throughout the observational period, is accounted for.

Although in the present observations the downslope propagating bore is not associated with large shear-induced Kelvin-Helmholtz billows as was observed in (also rare) flow over a promontory in the Gulf of Valencia [*van Haren et al.*, 2013], the presently observed convective instabilities create large turbulence. While there is some uncertainty to quantify this turbulence due to variation in the local temperature-density relationship, it is estimated to be at least of the same order of magnitude as in upslope propagating bores. An essential difference is the turbulence coming from the interior, rather than extending from the bottom upwards, and thus less affecting the resuspension of sediment. Given the rareness of occurrence of a downslope front compared to upslope propagating fronts, the latter seem to contribute more to overall turbulence generation by internal wave breaking over sloping topography, confirming previous estimates over seamounts [e.g., *van Haren and Gostiaux*, 2012]. However, despite its rareness, it is challenging to establish the precise nature of downslope propagating fronts in the future, with turbulent bursts in the form of stalagmites rather than stalactites (Fig. 1, lower-right). We note that the present observations were made in mid-summer, when mode- and deep-water formation are not known to occur.

Acknowledgments

We thank the captain and crew of the RRS James Cook and Colin Griffiths for their assistance in the mooring deployment. FASTNEt was funded by the UK Natural Environment Research Council through grant NE/I030232/1. NIOZ temperature sensors are supported by investment grants from the Netherlands organization for the advancement of scientific

research, NWO. Data use requests can be directed to hans.van.haren@nioz.nl or phil.hosegood@plymouth.ac.uk.

References

Allaby, A., M. Allaby (1999), *A Dictionary of Earth Sciences*, Oxford University Press, Oxford, UK.

Baines, P. G. (1982), On internal tide generation models, *Deep-Sea Res., 29*, 307-388.

Boubnov, B. M., and G. S. Golitsyn (1990), Temperature and velocity field regimes of convective motions in a rotating plane fluid layer, *J. Fluid Mech., 219*, 215-239.

Bourgault, D., M. Morsilli, C. Richards, U. Neumeier, D. E. Kelley (2014), Sediment resuspension and nepheloid layers induced by long internal solitary waves shoaling orthogonally on uniform slopes, *Cont. Shelf Res., 72*, 21-33.

Dauxois, T., A. Didier, and E. Falcon (2004), Observation of near-critical reflection of internal waves in a stably stratified fluid, *Phys. Fluids, 16*, 1936-1941.

Dillon, T. M. (1982), Vertical overturns: a comparison of Thorpe and Ozmidov length scales, *J. Geophys. Res., 87*, 9601-9613, doi:10.1029/JC087iC12p09601.

Eriksen, C. C. (1982), Observations of internal wave reflection off sloping bottoms, *J. Geophys. Res., 87*, 525-538.

Gemmrich, J. R., and H. van Haren (2001), Thermal fronts generated by internal waves propagating obliquely along the continental slope, *J. Phys. Oceanogr., 31*, 649-655.

Gerkema, T., F.-P. Lam, and L. R. M. Maas (2004), Internal tides in the Bay of Biscay: conversion rates and seasonal effects, *Deep-Sea Res. II, 51*, 2995-3008.

Gregg, M. C. (1989), Scaling turbulent dissipation in the thermocline, *J. Geophys. Res., 94*, 9686-9698.

Helfrich, K. R., 1992. Internal solitary wave breaking and run-up on a uniform slope, *J. Fluid Mech., 243*, 133-154.

Hosegood, P., and H. van Haren (2004), Near-bed solibores over the continental slope in the Faeroe-Shetland Channel, *Deep-Sea Res. II, 51*, 2943-2971.

Hosegood, P., J. Bonnin, and H. van Haren (2004), Solibore-induced sediment resuspension in the Faeroe-Shetland Channel, *Geophys. Res. Lett.*, *31*, L09301, doi:10.1029/2004GL019544.

IOC, SCOR, and IAPSO (2010), *The international thermodynamic equation of seawater – 2010: Calculation and use of thermodynamic properties*, Intergovernmental Oceanographic Commission, Manuals and Guides No. 56, UNESCO, Paris, France.

Klymak, J. M., and J. M. Moum (2003), Internal solitary waves of elevation advancing on a shoaling shelf, *Geophys. Res. Lett., 30*, 2045, doi:10.1029/2003GL017706.

Lawrie, A. G. W., and S. B. Dalziel (2011), Rayleigh-Taylor mixing in an otherwise stable stratification, *J. Fluid Mech., 688*, 507-527.

LeBlond, P. H., and L. A. Mysak (1978), *Waves in the ocean*, Elsevier, New York.

Lister, C. R. B. (1990), An explanation for the multivalued heat transport found experimentally for convection in a porous medium, *J. Fluid Mech., 214*, 287-320.

Marshall, J., and F. Schott (1999), Open-ocean convection: observations, theory, and models, *Rev. Geophys., 37*, 1-64.

Munk, W. (1997), Once again: once again—tidal friction. *Progr. Oceanogr., 40*, 7-35.

Oakey, N. S. (1982), Determination of the rate of dissipation of turbulent energy from simultaneous temperature and velocity shear microstructure measurements, *J. Phys. Oceanogr., 12*, 256-271.

Osborn, T. R. (1980), Estimates of the local rate of vertical diffusion from dissipation measurements, *J. Phys. Oceanogr., 10*, 83-89.RDI (1996), *Acoustic Doppler Current Profiler. Principles of Operation. A practical primer*, RD Instruments, San Diego.

Shrira, V. I. (1981), On the propagation of a three-dimensional packet of weakly non-linear internal gravity waves, *Int. J. Nonlin. Mech.*, *16*, 129-138.

Stashchuk, N., and V. Vlasenko (2017), Bottom trapped internal waves over the Malin Sea continental slope, *Deep-Sea Res.*, *119*, 68-80.

Thorpe, S. A. (1977), Turbulence and mixing in a Scottish loch, *Phil. Trans. Roy. Soc. Lond. A, 2*86, 125-181.

Thorpe, S. A. (1987), Transitional phenomena and the development of turbulence in stratified fluids: a review, *J. Geophys. Res., 92*, 5231-5248.

Thorpe, S. A. (1992), Thermal fronts caused by internal gravity waves reflecting from a slope, *J. Phys. Oceanogr., 22*, 105-108.

van Haren, H. (2006), Nonlinear motions at the internal tide source, *Geophys. Res. Lett., 33*, L11605, doi:10.1029/2006GL025851.

van Haren, H. (2007), Echo intensity data as a directional antenna for observing processes above sloping ocean bottoms, *Ocean Dyn., 57*, 135-149.

van Haren, H., and L. Gostiaux (2012), Detailed internal wave mixing observed above a deep-ocean slope, *J. Mar. Res., 70*, 173-197.

van Haren, H., M. Laan, D.-J. Buijsman, L. Gostiaux, M. G. Smit, and E. Keijzer (2009), NIOZ3: independent temperature sensors sampling yearlong data at a rate of 1 Hz, *IEEE J. Ocean. Eng., 34*, 315-322.

van Haren, H., M. Ribó, and P. Puig (2013), (Sub-)inertial wave boundary turbulence in the Gulf of Valencia, *J. Geophys. Res., 118*, 2067-2073, doi:10.1002/jgrc.20168.

van Haren, H., A. A. Cimatoribus, and L. Gostiaux, (2015), Where large deep-ocean waves break, *Geophys. Res. Lett*., *42*, 2351-2357, doi:10.1002/2015GL063329.

Venayagamoorthy, S. K., and O. B. Fringer (2012), On the formation and propagation of nonlinear internal boluses across a shelf break, *J. Fluid Mech., 577*, 137-159.

Vlasenko, V., and K. Hutter (2002), Numerical experiments on the breaking of solitary internal waves over a slope-shelf topography, *J. Phys. Oceanogr., 32*, 1779-1793.

Vlasenko, V., N. Stashchuk, M. E. Inall, and J. E. Hopkins (2014), Tidal energy conversion in a global hot spot: On the 3-D dynamics of baroclinic tides at the Celtic Sea shelf break, *J. Geophys. Res., 119*, 3249-3265, doi:10.1002/2013JC009708.

Figure 1. Sketch of upslope and downslope propagating fronts and hypothesized generation mechanisms. The thin solid arrows indicate the direction of (wave) propagation. The dashed arrow indicates the sequence in time.

Figure 2. Study area over the Malin continental slope. The temperature sensor mooring array is denoted by the yellow dot, where local water depth is about 200 m below that of the shelf break. The horizontal coordinate axes are indicated by [u, v]; the large open arrows indicate the slope current, as was also observed at other current meter moorings in the vicinity. Depth contours are drawn for 200, 500, 1000, 1500 and 2000 m.

Figure 3. Local shipborne CTD data <1 km from thermistor string mooring (black profile from 55° 53.783′N, 9°17.010′W, 378 m water depth, day 183.125) and down to 1030 m about 10 km offslope (blue profiles; 55° 55.155′N, 9°26.424′W, day 185.937). (a) Absolute Salinity, with horizontal scale equally contributing to density as the one in panel b. (b) Conservative Temperature. The purple bar indicates the range of the moored T-sensor array. (c) Relative density referenced to the surface. (d) Temperature-density relationship, with linear best-fits in red and purple for the data portions in the upper half of the water column. (e) Zoom of d, for the T-range of the moored sensors, with linear best-fit slopes indicated for the ranges 20-240 m (slope -0.2), 240-300 m (-0.6) and 300-378 m (-1). The blue profile slope of -0.23 is for the range 240-380 m.

Figure 4. Moored data overview for the entire 15 day period. (a) Conservative Temperature from high-resolution T-sensors. The purple vertical bars indicate the periods of Figures 5 and 6, respectively. The blue horizontal bars indicate the 27 lost sensors. (b) Cross-slope current component from ADCP. (c) Along-slope current component from ADCP. (d) Vertical current component from ADCP. (e) Relative echo amplitude from ADCP-beam 1.

Figure 5. As Figure 4, but for a 2 hour period around the passage of an example upslope propagating frontal bore; the temperature range is different and missing sensor data have been interpolated in a.

Figure 6. As Figure 5, but for a 2 hour period around the rare passage of a downslope propagating gravity current.

Figure 7. (a) Relative echo amplitude from ADCP-beams 1-4 during the downslope front with the time of arrival of the trailing edge at beams 1 and 2 indicated as t_1 and t_2, respectively. (b) A plan view of the ADCP heading and its 4 beams at the time relative to the bathymetric slope. (c) A side-on view of the downward looking ADCP indicating the 64 m horizontal distance between beams 1 and 2 at a range of 90 m.

Figure 1.

Upslope propagating internal front

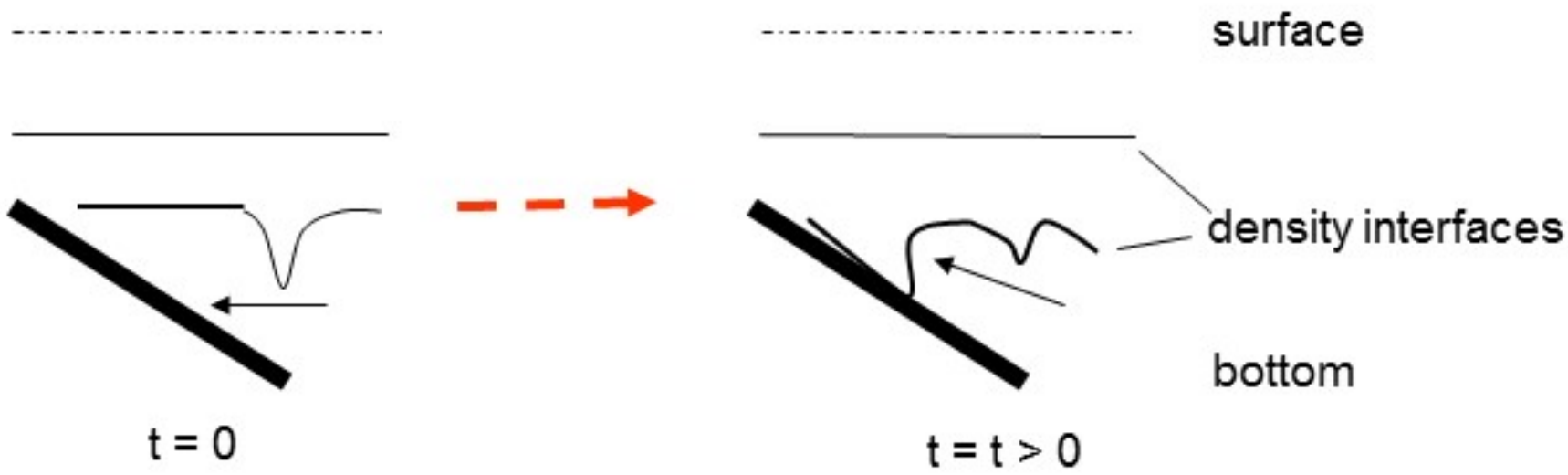

Downslope propagating front

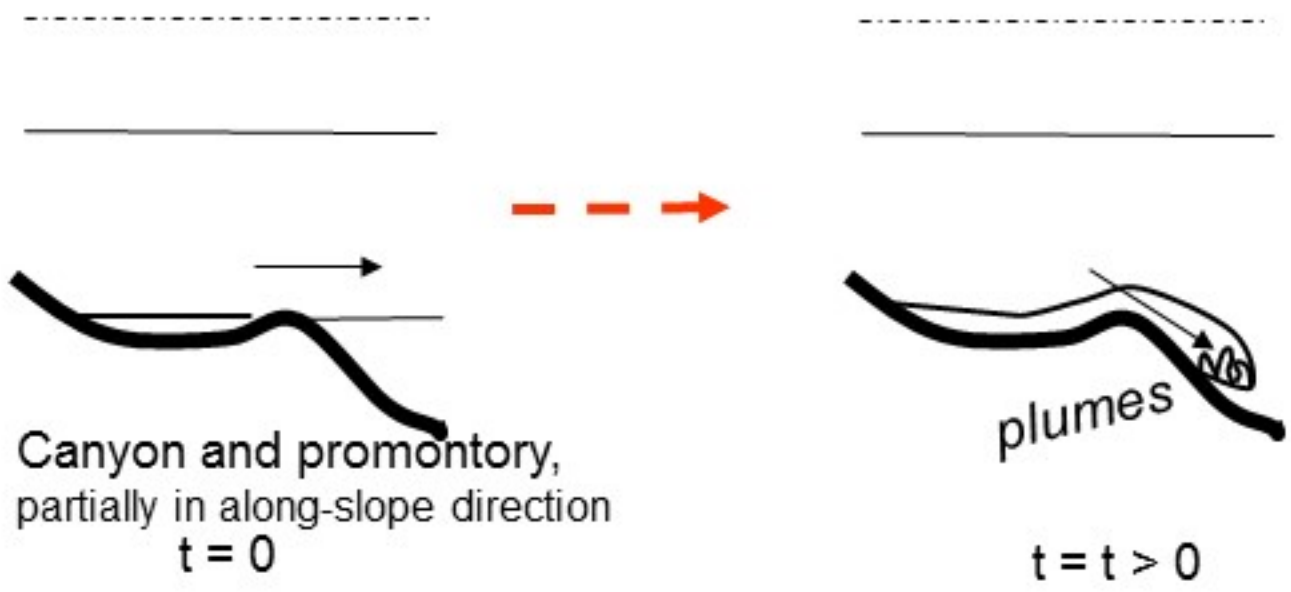

Figure 2.

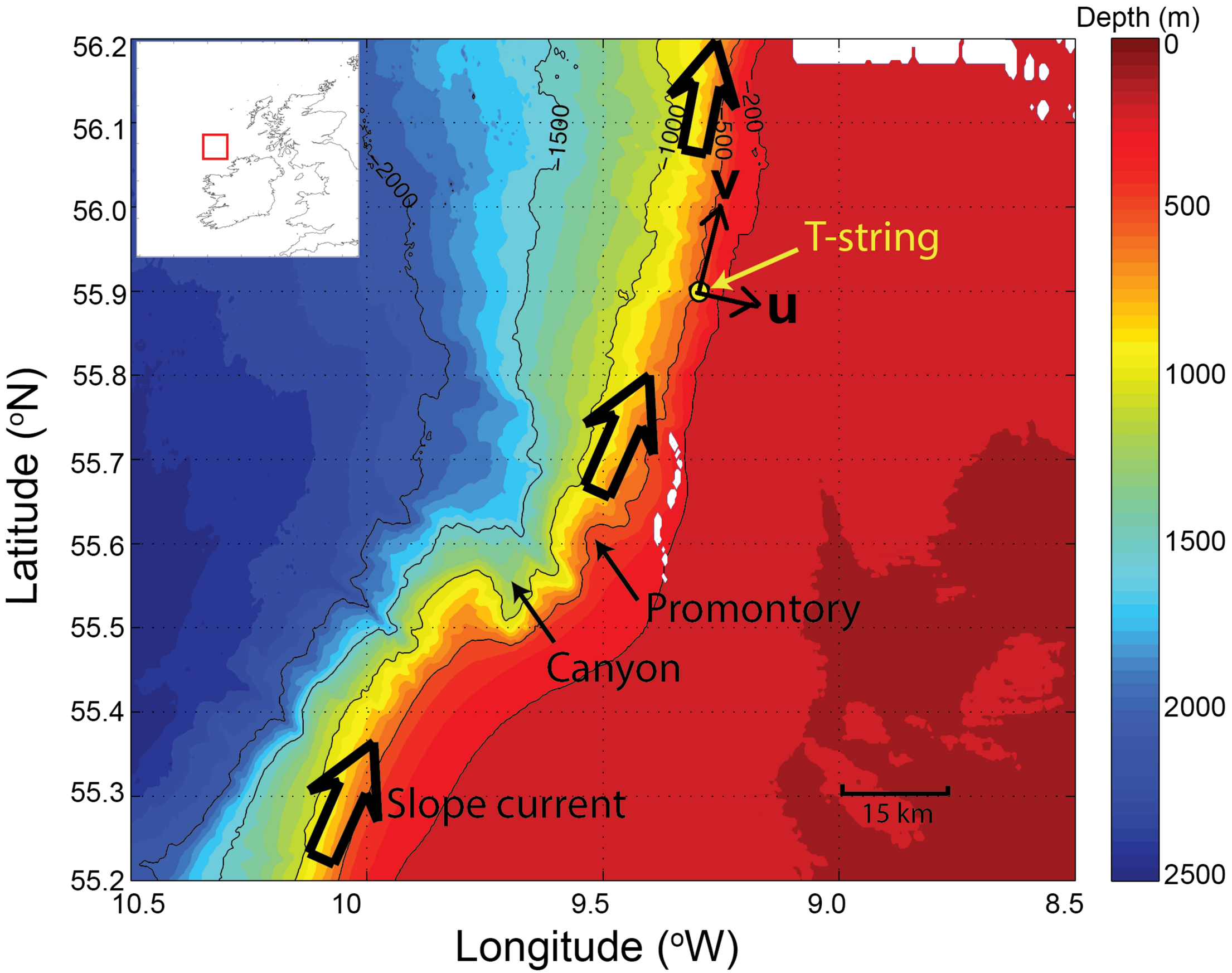

Figure 3.

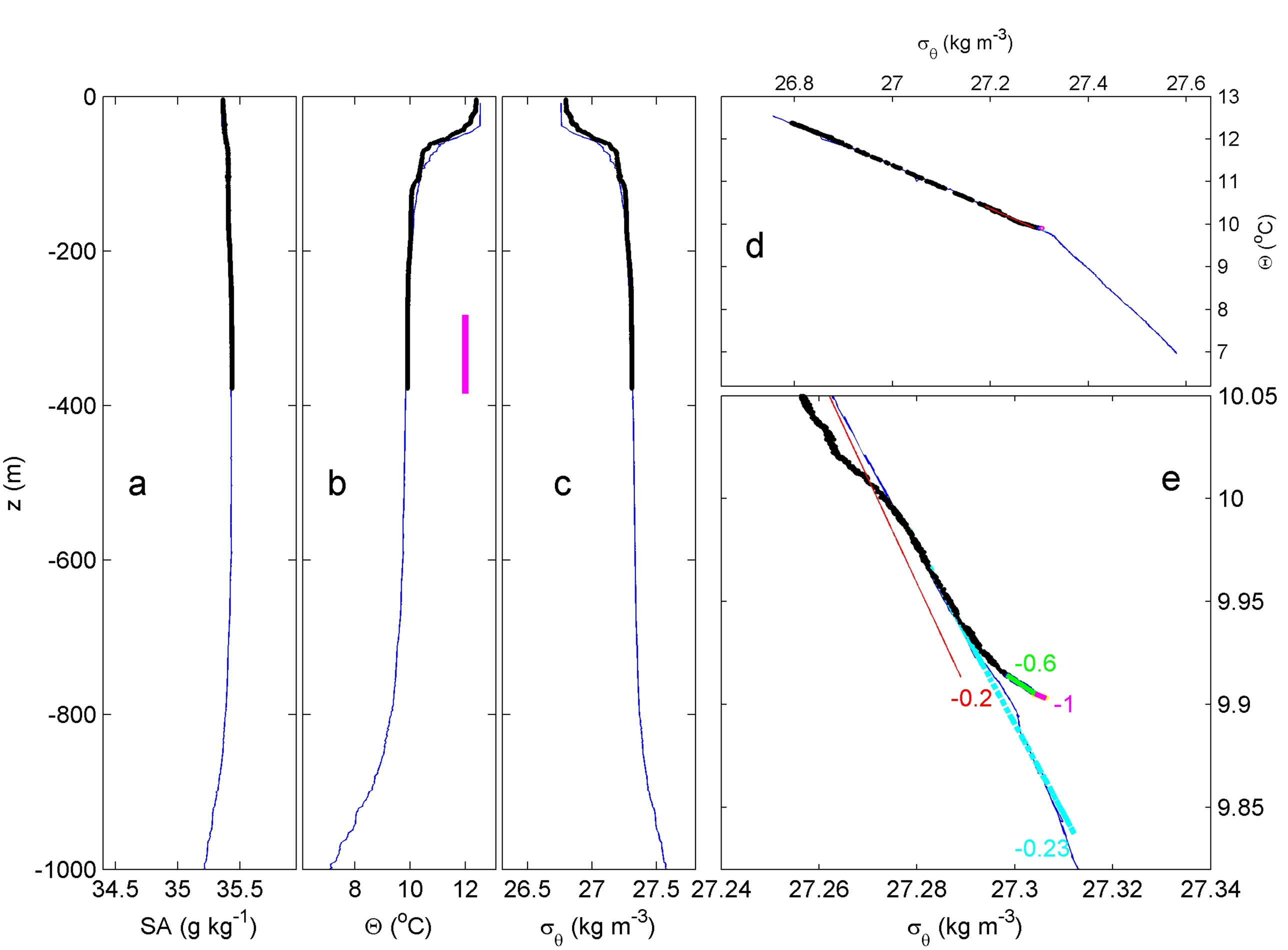

Figure 4.

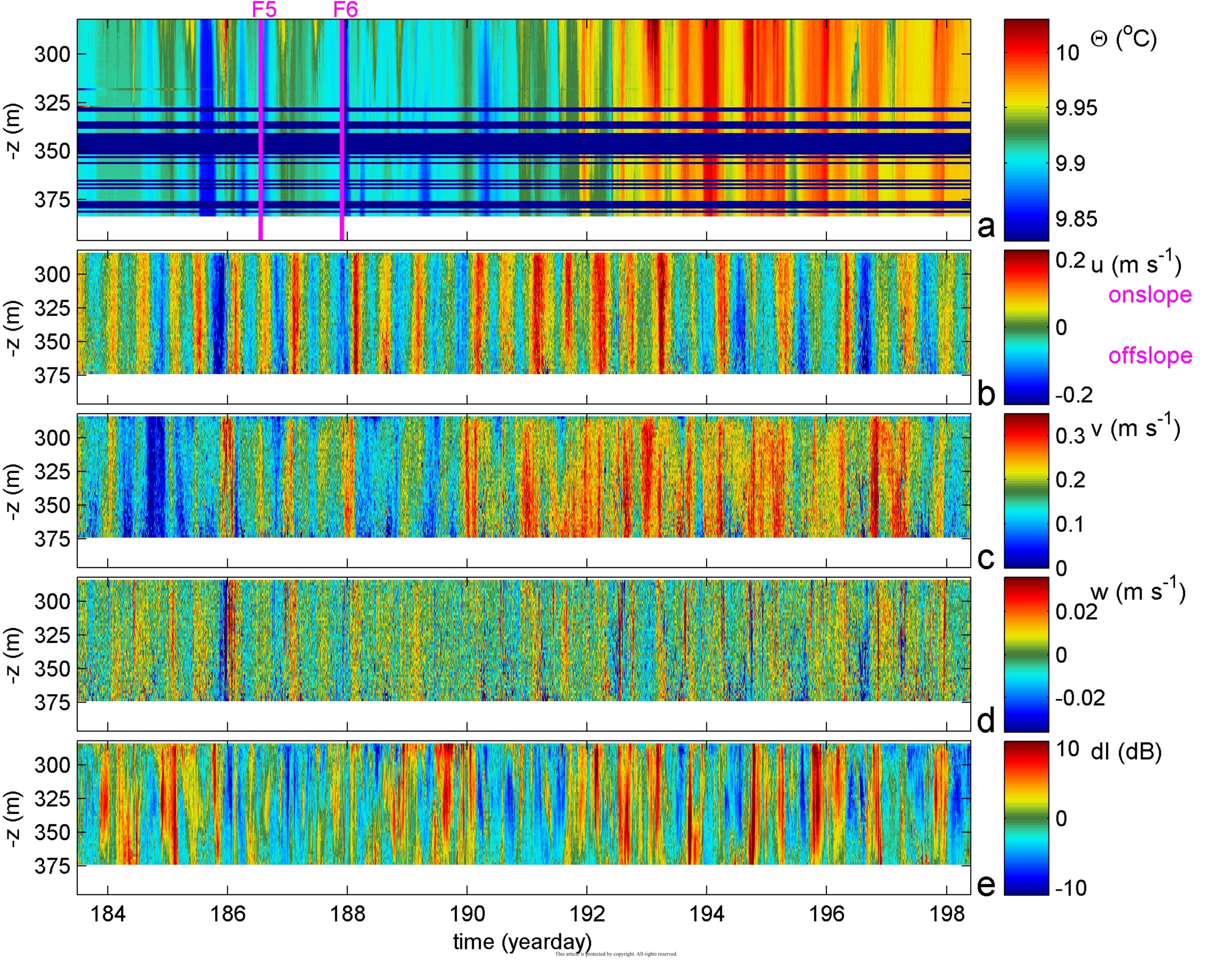

Figure 5.

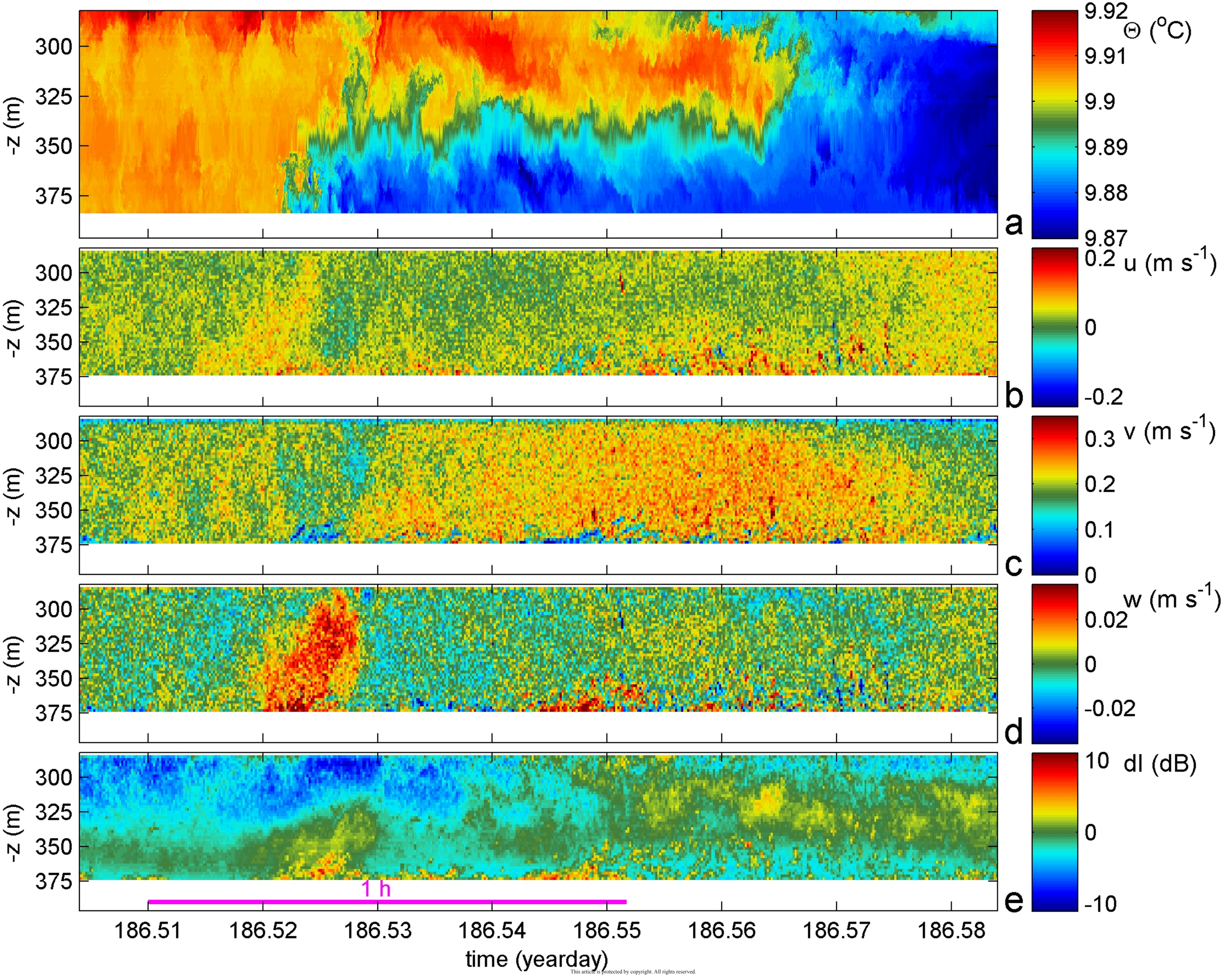

Figure 6.

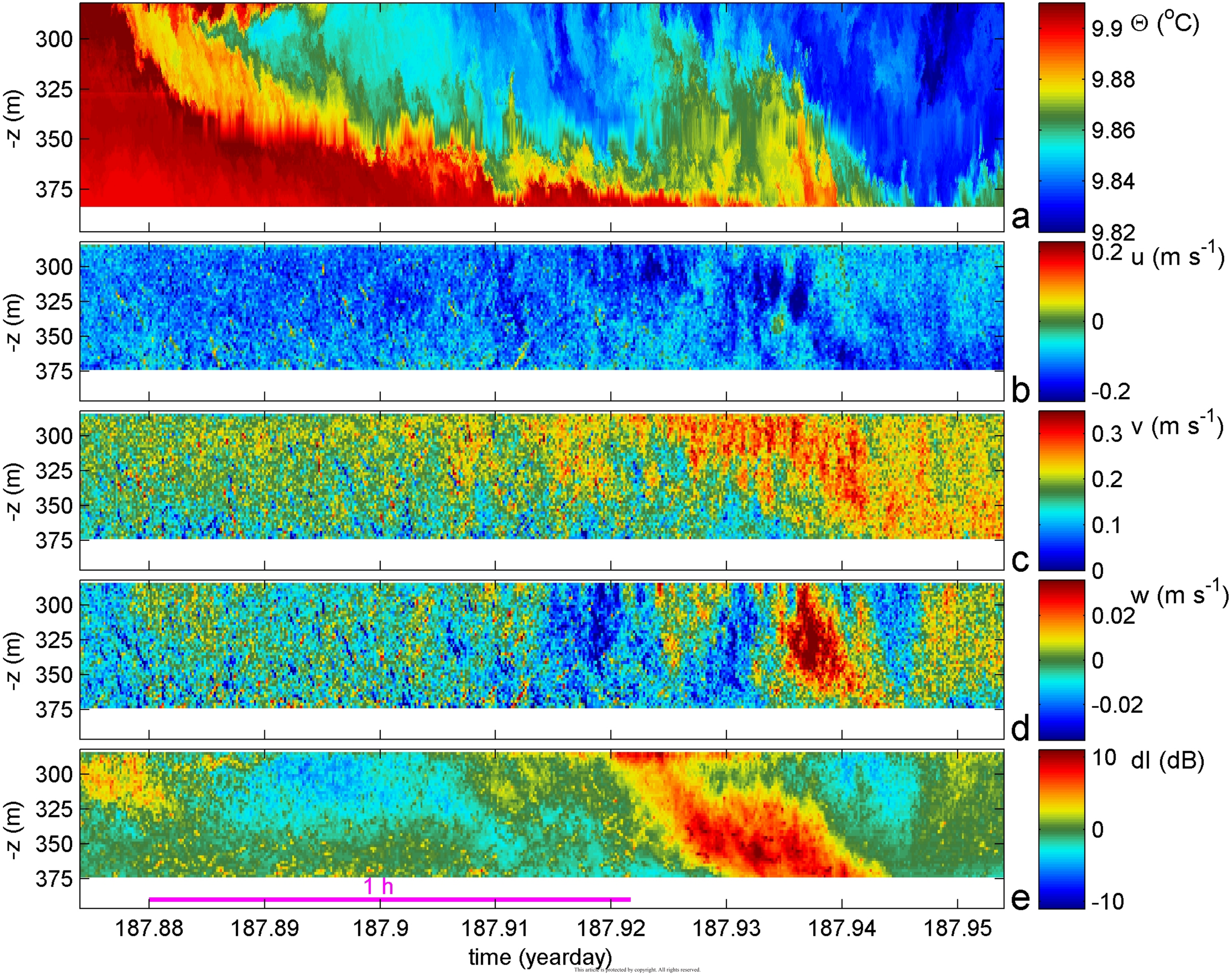

Figure 7.

a)

t_1 t_2

dI(dB)

Beam 1 2 3 4

-z (m)

280 300 320 340 360

187.91 187.915 187.92 187.925 187.93 187.935 187.94 187.945 187.95

10 0 -10

time (yearday)

b)

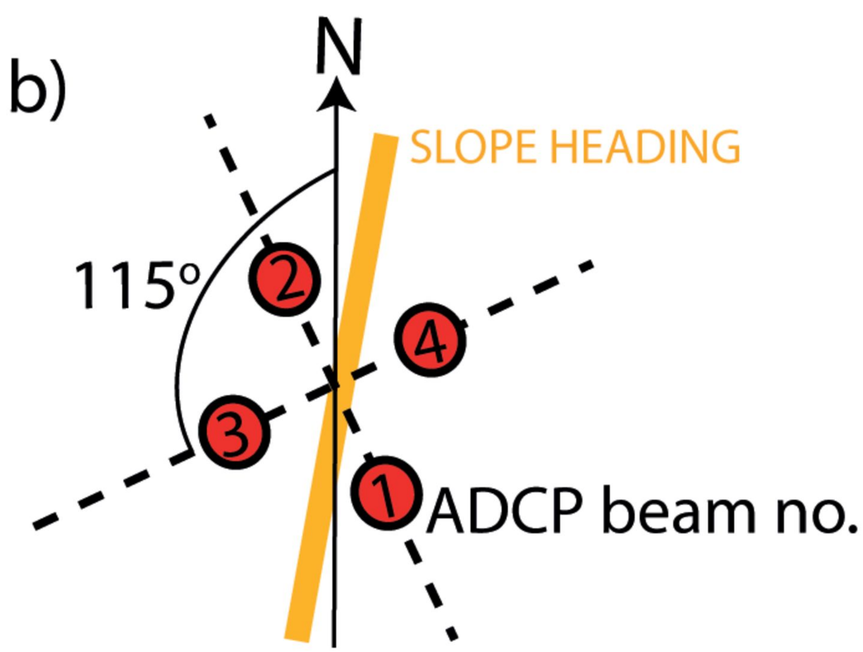

c)

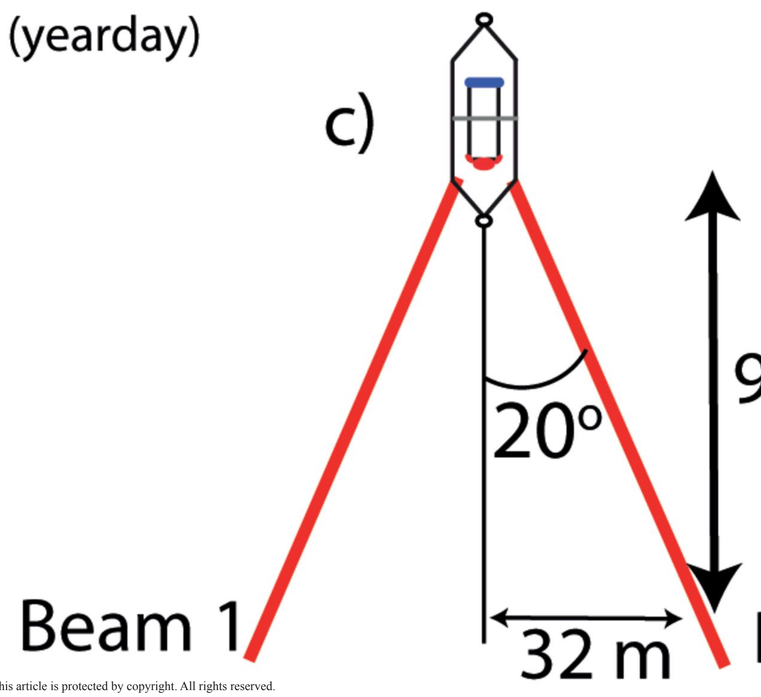

t_2-t_1 = 293 seconds

c = 64 m/293 s

= 0.21 m s^{-1}